Results in Physics 8 (2018) 524–531

Contents lists available at ScienceDirect

Results in Physics

journal homepage: www.journals.elsevier.com/results-in-physics

On radiative heat transfer in stagnation point flow of MHD Carreau fluid over a stretched surface

Masood Khan [a], Humara Sardar [a,*], M. Mudassar Gulzar [b]

[a] Department of Mathematics, Quaid-i-Azam University, Islamabad 44000, Pakistan
[b] Department of Basic Sciences and Humanities, College of Electrical and Mechanical Engineering, National University of Sciences and Technology, Islamabad 44000, Pakistan

ARTICLE INFO

Article history:
Received 26 October 2017
Received in revised form 13 December 2017
Accepted 16 December 2017
Available online 20 December 2017

Keywords:
Magnetohydrodynamic flow
Carreau viscosity model
Stagnation point flow
Heat transfer analysis
Non-linear radiation
Joule heating
Numerical computations

ABSTRACT

This paper investigates the behavior of MHD stagnation point flow of Carreau fluid in the presence of infinite shear rate viscosity. Additionally heat transfer analysis in the existence of non-linear radiation with convective boundary condition is performed. Moreover effects of Joule heating is observed and mathematical analysis is presented in the presence of viscous dissipation. The suitable transformations are employed to alter the leading partial differential equations to a set of ordinary differential equations. The subsequent non-straight common ordinary differential equations are solved numerically by an effective numerical approach specifically Runge-Kutta Fehlberg method alongside shooting technique. It is found that the higher values of Hartmann number (M) correspond to thickening of the thermal and thinning of momentum boundary layer thickness. The analysis further reveals that the fluid velocity is diminished by increasing the viscosity ratio parameter (β^*) and opposite trend is observed for temperature profile for both hydrodynamic and hydromagnetic flows. In addition the momentum boundary layer thickness is increased with velocity ratio parameter (α) and opposite is true for thermal boundary layer thickness.

Introduction

Now a days flows of non-Newtonian liquids in the presence of magnetic field have significant role in a number of industrial and engineering processes. The common examples of such magneto fluids include plasmas, salt water and electrolytes. The basic concept behind magnetohydrodynamics is that magnetic fields can induce currents in a moving conductive fluid, which in turn polarizes the fluid and reciprocally changes the magnetic field itself. The pioneer work on MHD flow past a stretching surface was done by Palov [1]. After that Andersson [2] inspected the MHD flow of a viscous fluid. Moreover Makinde et al. [3] discovered the MHD variable viscosity flow over a convectively heated plate in porous medium along thermophoresis and radiative heat transfer. Few latest studies in this direction can be seen through the attempts [4–6]. Sakiadis [7] discussed the boundary layer behavior on a moving surface and he applied similarity transformations to the boundary layer equations and then numerically solved. Crane [8] simplified the work of Sakiadis.

Thermal radiation is one of the key components of heat exchange. It is produced by the thermal motion of charged particles in matter. All matter with a temperature greater than absolute zero emits thermal radiation. Heat transfer analysis with radiation plays an important role in industrial and technological process. This contains the design of furnace, heat exchangers, safety of nuclear reactor, power plants and turbid water bodies [9]. Various discoveries have been accounted on the boundary layer flows in the stagnation point region. Stagnation points have huge applications in real world and mechanical procedures. These procedures incorporate blowing glass, drying and cooling of papers and other mechanical procedures in designing. The steady two dimensional flow with stagnation point in an incompressible micro polar fluid over a stretching sheet has been studied by Nazar et al. [10]. Farooq et al. [11] studied the stagnation point flow with MHD in a viscoelastic nano fluid with non-linear radiation effects. Heat transfer with porous medium over a stretching sheet with thermal radiation and variable thermal conductivity was discussed by Cortell [12]. Moreover, a numerical examination of heat transfer and flow of Carreau fluid in cylindrical coordinates was discovered by Khellaf and Lauriat [13]. Effect of Carreau fluid flow down an inclined plane with a free surface was inspected by Tshehla [14]. Abbasi et al. [15] discovered the MHD peristaltic transport of Carreau fluid in curved channel with Hall effects.

* Corresponding author.
E-mail address: humarasardar@math.qau.edu.pk (H. Sardar).

https://doi.org/10.1016/j.rinp.2017.12.046
2211-3797/

Further, the impact of thermal radiation is important in space innovation and high temperature forms. Hossain et al. [16] explored the thermal radiation's effects with the Rosseland diffusion approximation on convective flow over a vertical uniformly heated porous plate. Later on, Hayat et al. [17] inspected the MHD three dimensional flow of a nano fluid with nonlinear thermal radiation and velocity slip. Also Hayat et al. [18] discussed the Oldroyd-B nanofluid flow with MHD over a stretching sheet with heat generation/absorption. Recently Khan and Hashim [19] explored the MHD flow with stagnation point and heat transfer in Carreau fluid along with convective boundary conditions. Additionally, Khan et al. [20] investigated the Carreau fluid with MHD over a convectively heated surface with nonlinear radiation. Advancements in the study of non-Newtonian fluids have been made by different authors [27–31].

The aim of the present study is to address the effects of the MHD Carreau fluid in stagnation point flow with infinite shear rate viscosity. Additionally, Joule heating and nonlinear radiative heat transfer is studied in the presence of convective boundary condition. It is important to note that Carreau fluid is a distinct class of generalized Newtonian fluid which classifies shear thinning and shear thickening nature of fluids. The governing partial differential equations are converted to a set of non-linear ordinary differential equations. Then are solved numerically by applying Runge-Kutta fourth-fifth order method via shooting technique. Current research graphically presents the physical importance of the parameters on the temperature and velocity profiles. The influences of the pertinent flow variables M, α, β^*, N_R, θ_w and γ are described through tables and graphs.

Mathematical formulation

We examine the steady boundary layer flow of an incompressible Carreau viscosity liquid model in the region of stagnation point near a stretching surface. The flow is initiated by a linear stretching surface. The coordinate system is designated in such a way that x-axis is measured alongside the stretching sheet while y-axis is normal to it and fluid conquers the space $y > 0$. The magnetic field B_0 is uniform and applied in y direction and the induced magnetic field is neglected under low magnetic Reynolds number assumption. The sheet velocity is assumed to be $u_w(x) = cx$ with $c > 0$ is stretching rate. The velocity of exterior flow is $u_\infty = ax$ $(a > 0)$, where a is constant. Moreover, heat transfer analysis is completed along the nonlinear thermal radiation with convective boundary condition at the surface. The viscous dissipation and Joul heating effects are also incorporated (Fig. 1).

The constitutive equations for the generalized Newtonian Carreau fluid [20,21] are given as

$$\boldsymbol{\tau} = -p\mathbf{I} + \mu(\dot{\gamma})\mathbf{A}_1, \quad \mu = \mu_0\left[\beta^* + (1-\beta^*)[1+(\Gamma\dot{\gamma})^2]^{\frac{n-1}{2}}\right]. \tag{1}$$

Here $\boldsymbol{\tau}$ is the Cauchy stress tensor, p the pressure, $\mathbf{A}_1$ the first Rivlin-Erickson tensor, $\mathbf{I}$ the identity tensor, $\dot{\gamma} = \sqrt{\frac{1}{2}\Pi}$ with Π as the second invariant strain tensor and defined as $\Pi = trace(\mathbf{A}_1^2)$, n the power law index, Γ a material time constant and $\beta^* = (\mu_\infty/\mu_o)$ the viscosity ratio parameter with μ_0 the zero shear rate viscosity, μ_∞ the infinite shear rate viscosity and taken to be less than one here.

Under the above assumptions and the usual boundary-layer approximations, the governing boundary layer equations for present flow are given by

$$\frac{\partial u}{\partial x} + \frac{\partial v}{\partial y} = 0, \tag{2}$$

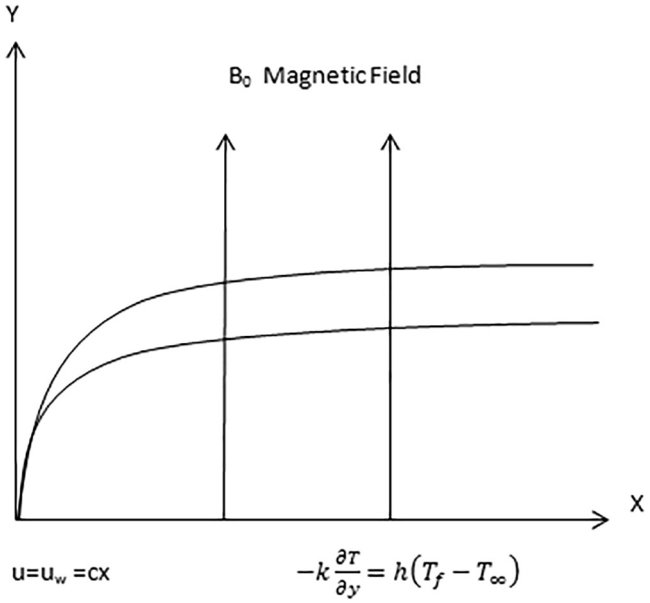

Fig. 1. Physical model under consideration.

$$u\frac{\partial u}{\partial x} + v\frac{\partial u}{\partial y} = u_\infty\frac{du_\infty}{dx} + \nu\left(\frac{\partial^2 u}{\partial y^2}\right)\left[\beta^* + (1-\beta^*)\left\{1+\Gamma^2\left(\frac{\partial u}{\partial y}\right)^2\right\}^{\frac{n-1}{2}}\right] + \nu(n-1)(1-\beta^*)\Gamma^2\left(\frac{\partial^2 u}{\partial y^2}\right)\left(\frac{\partial u}{\partial y}\right)^2\left\{1+\Gamma^2\left(\frac{\partial u}{\partial y}\right)^2\right\}^{\frac{n-3}{2}} + \frac{\sigma B_0^2}{\rho}(u_\infty - u), \tag{3}$$

$$u\frac{\partial T}{\partial x} + v\frac{\partial T}{\partial y} = \alpha_1\frac{\partial^2 T}{\partial y^2} - \frac{1}{\rho c_p}\frac{\partial q_r}{\partial y} + \frac{\sigma B_0^2}{\rho c_p}u^2 + \frac{\nu}{c_p}\left(\frac{\partial u}{\partial y}\right)^2\left[\beta^* + (1-\beta^*)\left\{1+\Gamma^2\left(\frac{\partial u}{\partial y}\right)^2\right\}^{\frac{n-1}{2}}\right]. \tag{4}$$

In the above equations, $\alpha_1 = \frac{k}{\rho c_p}$ is the thermal diffusivity with c_p the specific heat and k the thermal conductivity, σ the electrical conductivity of the fluid and $\nu = \frac{\mu_0}{\rho}$ the kinematic viscosity of the base fluid.

Note that fluid is portrayed as Newtonian fluid for $n = 1$ and/or $\Gamma = 0$, shear thinning for $0 < n < 1$ and shear thickening for $n > 1$.

Radiative heat flux used in Eq. (4) is given by the Roseland approximation [22]

$$q_r = -\left(\frac{4\sigma^*}{3k^*}\frac{\partial T^4}{\partial y}\right), \tag{5}$$

where σ^* and k^* are the Stefan-Boltzman constant and the mean absorption coefficient, respectively. For a planer boundary layer flow over a heated surface, Eq. (5) can be written as [23]

$$q_r = -\frac{16\sigma^*}{3k^*}\left(T^3\frac{\partial T}{\partial y}\right). \tag{6}$$

Using Eq. (6) the energy Eq. (4) can be composed as

$$u\frac{\partial T}{\partial x} + v\frac{\partial T}{\partial y} = \frac{\partial}{\partial y}\left[\left(\alpha + \frac{16\sigma^*}{3k^*}\frac{T^3}{\rho c_p}\right)\frac{\partial T}{\partial y}\right] + \frac{\sigma B_0^2}{\rho c_p}u^2 + \frac{\nu}{c_p}\left(\frac{\partial u}{\partial y}\right)^2\left[\beta^* + (1-\beta^*)\left\{1+\Gamma^2\left(\frac{\partial u}{\partial y}\right)^2\right\}^{\frac{n-1}{2}}\right]. \tag{7}$$

The boundary conditions of the present problem are

$$u = u_w = cx, \quad v = 0, \quad -k\frac{\partial T}{\partial y} = h_f(T_f - T) \quad \text{at} \quad y = 0, \tag{8}$$

$$u = u_\infty \to ax, \quad T \to T_\infty \quad \text{as} \quad y \to \infty. \tag{9}$$

The following dimensionless quantities are utilized to change the governing partial differential equations into a scheme of ordinary differential equations

$$\eta = y\sqrt{\frac{c}{\nu}}, \quad \Psi(x,y) = x\sqrt{c\nu}f(\eta), \quad \theta(\eta) = \frac{T - T_\infty}{T_f - T_\infty}, \tag{10}$$

where Ψ denotes the stream function that satisfies equation of continuity with $u = \frac{\partial \Psi}{\partial y}$ and $v = -\frac{\partial \Psi}{\partial x}$. Also $T = T_\infty + [1 + (\theta_w - 1)\theta]$ where T_∞ is the ambient fluid temperature with $\theta_w = \frac{T_f}{T_\infty}$. Here $\theta_w (> 1)$ is the temperature ratio parameter.

Consequently, the momentum and energy equations with the relevant boundary conditions lessen to the accompanying ordinary differential equations

$$\left[\beta^* + (1-\beta^*)\left\{1 + We^2(f'')^2\right\}^{\frac{n-3}{2}}\left\{1 + nWe^2(f'')^2\right\}\right]f''' + ff'' - (f')^2 + \alpha^2 + M^2(\alpha - f') = 0, \tag{11}$$

$$\theta'' + \Pr f\theta' + \frac{4}{3N_R}\frac{d}{d\eta}\left[\{1 + (\theta_w - 1)\theta\}^3\theta'\right] + \Pr Ec(f'')^2\left[\beta^* + (1-\beta^*)\left\{1 + We^2(f'')^2\right\}^{\frac{n-1}{2}}\right] + M^2 \Pr Ec(f')^2 = 0, \tag{12}$$

with

$$f(0) = 0, \quad f'(0) = 1, \quad \theta'(0) = -\gamma[1 - \theta(0)], \tag{13}$$

$$f'(\infty) \to \alpha, \quad \theta(\infty) \to 0, \tag{14}$$

where prime denotes the differentiation with respect to variable η, $M = \sqrt{\frac{\sigma B_0^2}{\rho c}}$ is the Hartmann number, $\alpha = a/c$ the velocity ratio parameter, $We = \sqrt{\frac{c^3\Gamma^2x^2}{\nu}}$ the local Weissenberg number, $Pr = \frac{\mu c_p}{k}$ the Prandtl number, $N_R = \frac{kk^*}{4\sigma^* T_\infty^3}$ the radiation parameter, $Ec = \frac{(cx)^2}{c_p(T_f - T_\infty)}$ the Eckert number and $\gamma = \frac{h}{k}\sqrt{\frac{\nu}{c}}$ the local Biot number.

The local skin friction coefficient and the local Nusselt number are the parameters of engineering interest which characterize the surface drag and wall heat transfer. These parameters are defined as

$$C_{fx} = \frac{\tau_w}{\rho u_w^2(x)}, \quad Nu_x = \frac{xq_w}{k(T_f - T_\infty)}, \tag{15}$$

where τ_w is the surface shear stress and q_w the surface heat flux given by

$$\tau_w = \mu_0\left(\frac{\partial u}{\partial y}\right)\left[\beta^* + (1-\beta^*)\left\{1 + \Gamma^2\left(\frac{\partial u}{\partial y}\right)^2\right\}^{\frac{n-1}{2}}\right],$$
$$q_w = -k\left(\frac{\partial T}{\partial y}\right)_w + (q_r)_w. \tag{16}$$

Upon using Eq. (16), the local skin friction coefficient and local Nusselt number become

$$\mathrm{Re}^{1/2}C_{fx} = f''(0)\left[\beta^* + (1-\beta^*)\left\{1 + We^2(f''(0))^2\right\}^{\frac{n-1}{2}}\right],$$
$$\mathrm{Re}^{-1/2}Nu_x = -\theta'(0)\left\{1 + \frac{4}{3N_R}[1 + (\theta_w - 1)\theta(0)]^3\right\}. \tag{17}$$

where $\mathrm{Re}_x = \frac{xu_w}{\nu}$ is the local Reynolds number.

Solution methodology

The governing flow equations (Eqs. (11) and (12)) are highly nonlinear and partially coupled set of ordinary differential equations. In order to find solution of these equations along side boundary conditions (13)–(14), the shooting technique along with fourth-fifth order Runge-Kutta integration scheme is utilized. Since Runge-Kutta Fehlberg method solves only initial value problem. So firstly Eqs. (11) and (12) are converted into set of first order equations. For this purpose, we rewrite the above set of equations as given below:

$$f''' = \frac{(f')^2 - \alpha^2 - ff'' - M^2(\alpha - f')}{\left[\beta^* + (1-\beta^*)\left\{1 + nWe^2(f'')^2\right\}\left\{1 + We^2(f'')^2\right\}^{\frac{n-3}{2}}\right]}, \tag{18}$$

$$\theta'' = -\Pr f\theta' - \frac{4}{3N_R}\frac{d}{d\eta}\left[\{1 + (\theta_w - 1)\theta\}^3\theta'\right] - \Pr Ec(f'')^2\left[\beta^* + (1-\beta^*)\left\{1 + We^2(f'')^2\right\}^{\frac{n-1}{2}}\right] - M^2 \Pr Ec(f')^2. \tag{19}$$

The new variables defined below are utilized to reduce above higher order equations into system of first order differential equations:

$$f = y_1, \quad f' = y_2, \quad f'' = y_3, \quad f''' = y_3',$$
$$\theta = y_4, \quad \theta' = y_5, \quad \theta'' = y_5'. \tag{20}$$

After inserting Eq. (20) into Eqs. (18) and (19), a new system of first-order ordinary differential equations is obtained as:

$$y_1' = y_2, \quad y_2' = y_3, \quad y_3' = \frac{\left[y_2^2 - y_1y_3 - \alpha^2 - M^2(\alpha - y_2)\right]}{\beta^* + (1-\beta^*)\left[1 + nWe^2y_3^2\right]\left[1 + We^2y_3^2\right]^{\frac{n-3}{2}}}, \tag{21}$$

$$y_4' = y_5, \tag{22}$$

$$y_5' = \frac{-3\Pr N_R y_1y_5 - 12(\theta_w - 1)[1 + (\theta_w - 1)y_4]^2y_5^2}{3N_R + 4[1 + (\theta_w - 1)y_4]^3} - \frac{3N_R \Pr Ec(y_3)^2\left[\beta^* + (1-\beta^*)\left\{1 + We^2(y_3)^2\right\}^{\frac{n-1}{2}}\right] + M^2 \Pr Ec(y_2)^2}{3N_R + 4[1 + (\theta_w - 1)y_4]^3} \tag{23}$$

together with the boundary conditions

$$\begin{pmatrix} y_1 \\ y_2 \\ y_3 \\ y_4 \\ y_5 \end{pmatrix} = \begin{pmatrix} 0 \\ 1 \\ u_1 \\ u_2 \\ -\gamma(1 - u_2) \end{pmatrix}. \tag{24}$$

where u_1 and u_2 are the initial guesses for the $f''(0)$ and $\theta'(0)$.

The RK-Fehlberg method is an iterative algorithm which tries to find appropriate initial conditions for related initial value problem. For our problem, computations are based on the following steps:

Table 1
Contrast values of $-f''(0)$ for different α when $\beta^* = We = M = 0$ and $n = 1$.

α	Mahapatra and Gupta [24]	Nazar et al. [25]	Ishak et al. [26]	Present results
0.01	–	–	0.9980	0.998028
0.10	0.9694	0.9694	0.9694	0.969650
0.20	0.9181	0.9181	0.9181	0.918165
0.50	0.6673	0.6673	0.6673	0.667686

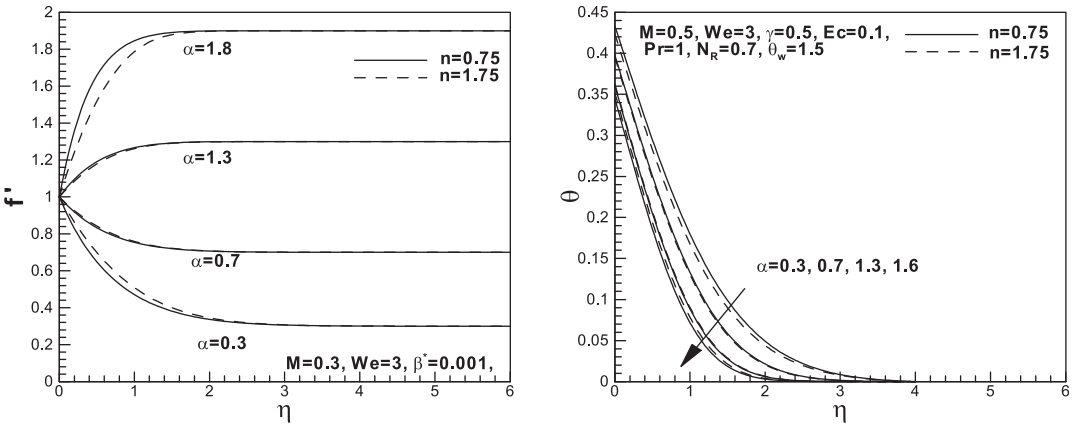

Fig. 2. Effects of the velocity ratio parameter α on the velocity and temperature distributions.

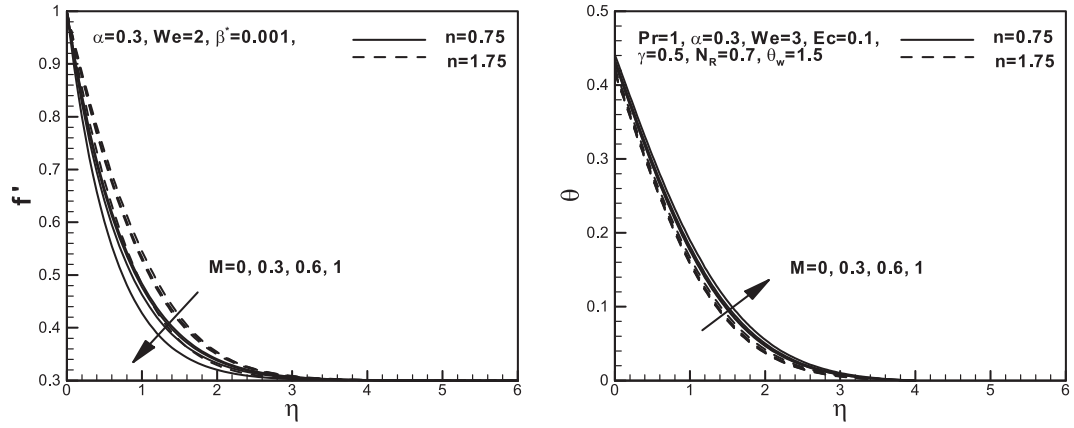

Fig. 3. Effects of the Hartmann number M on the velocity and temperature distributions.

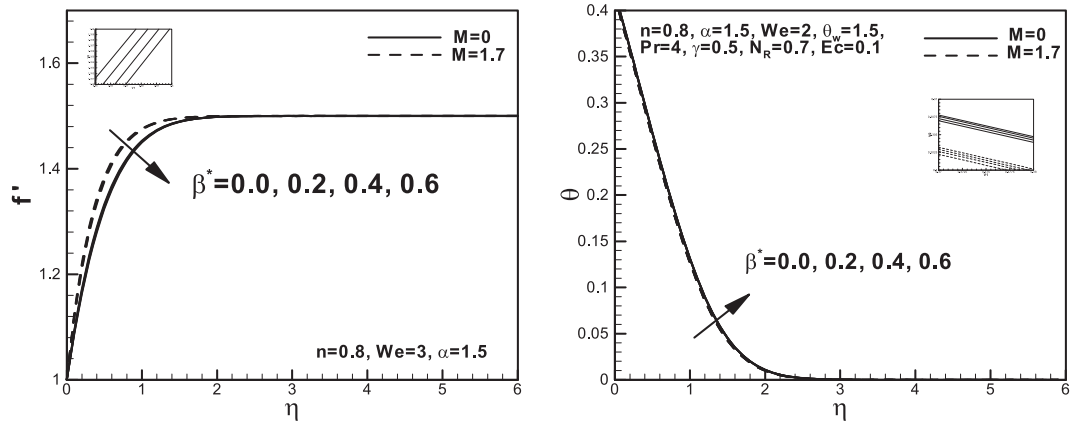

Fig. 4. Effects of the viscosity ratio parameter β^* on the velocity and temperature distributions.

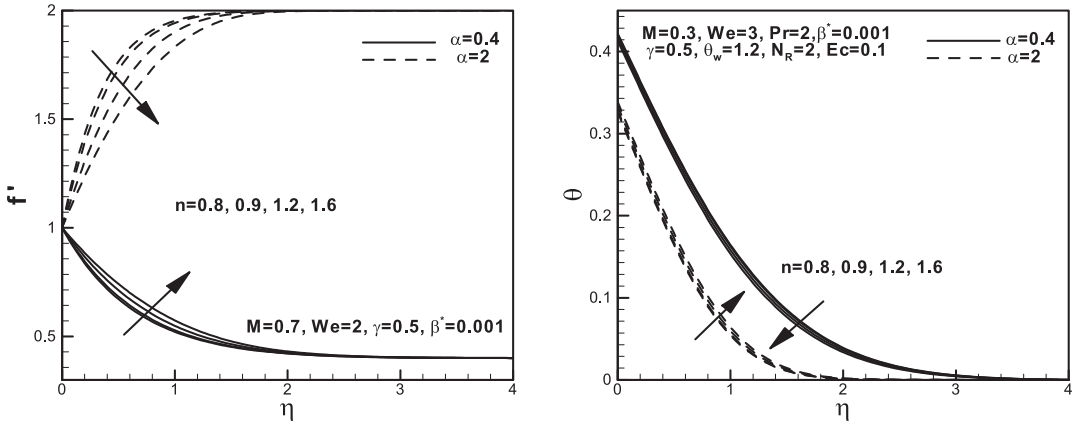

Fig. 5. Effects of the power law index n on the velocity and temperature distributions.

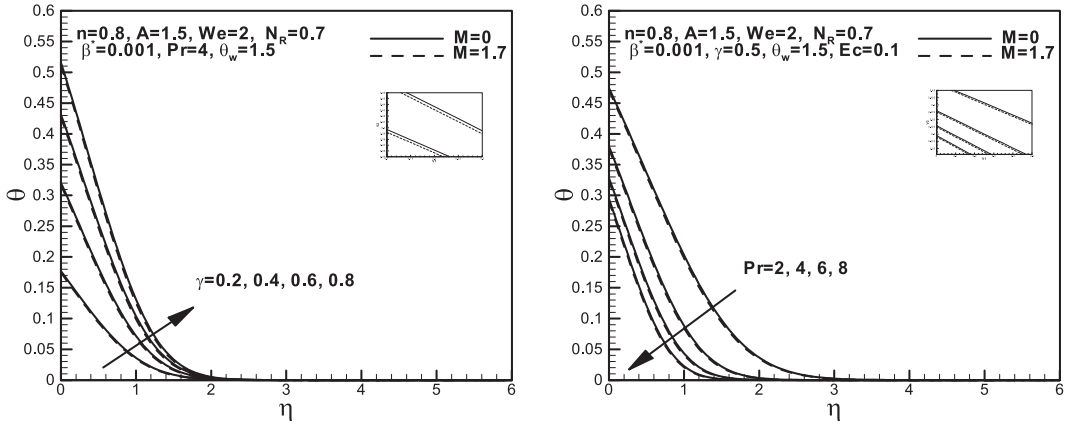

Fig. 6. Effects of the Biot number γ and Prandtl number Pr on the temperature distribution.

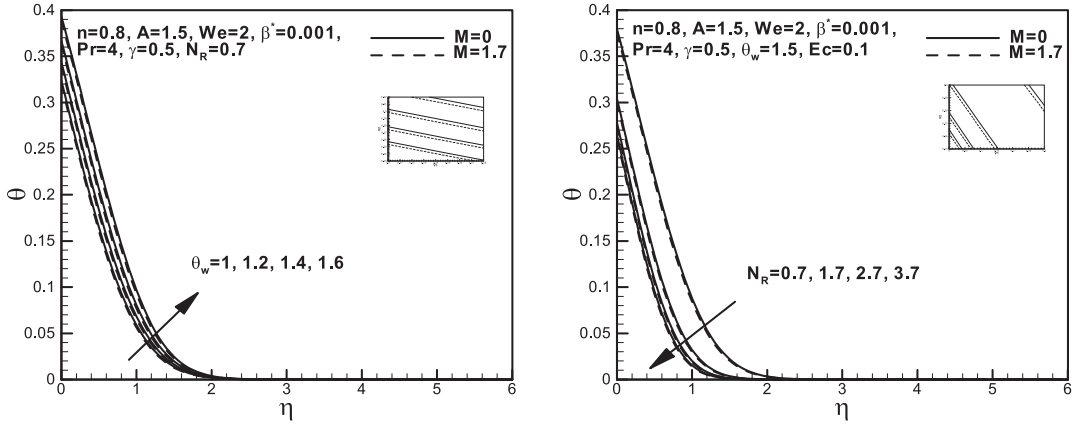

Fig. 7. Effects of the temperature ratio parameter θ_w and radiation parameter N_R on temperature distribution.

1. Firstly chose the limit of η_∞ and the best suited limit for η_∞ is between 5 to 10.
2. Then select suitable initial guesses for $y_3(0)$ and $y_4(0)$. Initially $y_3(0) = -1$ and $y_4(0) = 0.5$ are selected.
3. Then set of ODEs are solved with the help of fourth-fifth order Runge-Kutta integration scheme.
4. Finally, boundary residuals (absolute variations in given and calculated values of $y_2(\infty)$ and $y_4(\infty)$) is calculated. The solution will converge if entire values of boundary residuals are less then tolerance error, which is considered 10^{-5}.
5. If values of boundary residuals are larger than tolerance error, then values of $y_3(0)$ and $y_4(0)$ will be modified by Newton's method.

Result and discussion

In order to examine results of the present study a numerical computation is performed for MHD stagnation point flow of Carreau fluid with infinite shear rate viscosity and nonlinear radiation over a convectively heated surface. The partially coupled

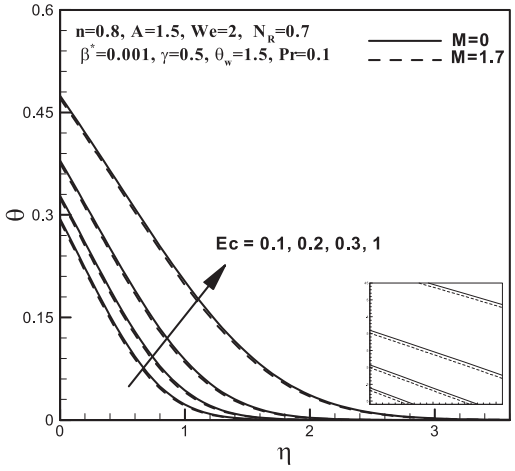

Fig. 8. Effects of the Eckert number *Ec* on temperature distribution.

set of Eqs. (11)–(12) with boundary conditions (13) and (14) are tackled numerically using Runge-Kutta fourth-fifth order method along with shooting technique. Moreover, representative outcomes about the skin friction and local Nusselt number are recorded through tables. The influence of non-dimensional parameters like α, M, β^*, n, γ, Pr, Ec, θ_w and N_R on dimensionless fluid velocity and temperature distributions are determined and presented through graphs. Additionally the accuracy of our numerical results is verified with earlier published results by Mahapatra and Gupta [24], Nazar et al. [25] and Ishak et al. [26] for particular cases through Table 1. A good agreement is reported between these results.

Fig. 2 represents a considerable variation in the velocity $f'(\eta)$ and the corresponding boundary layer thickness at points where free stream velocity is different from sheet velocity. It is noted that the velocity increases and the boundary layer thickness decreases with an increase in α for both shear thinning and thickening cases. Additionally increasing value of α depicts a significantly decrement in temperature $\theta(\eta)$. Fig. 3 is plotted to inspect the impact of Hartmann number M on temperature $\theta(\eta)$ and velocity $f'(\eta)$

Table 2
Surface drag force $Re^{1/2}C_{fx}$ and heat transfer rate $Re^{-1/2}Nu_x$ for different values of β^*, M, We and α when $\Pr = 1.5$, $\gamma = 0.3$, $\theta_w = 1.5$, $Ec = 0.1$ and $N_R = 1$.

M	We	α	β^*	$Re^{1/2}C_{fx}$		$Re^{-1/2}Nu_x$	
				$n = 0.75$	$n = 1.75$	$n = 0.75$	$n = 1.75$
0	3	0.3	0.001	−0.784896	−1.053800	0.500565	0.502467
0.3				−0.806517	−1.090060	0.500368	0.502376
0.6				−0.867699	−1.194930	0.499803	0.502112
0.8				−0.926226	−1.298290	0.499255	0.501852
0.3	2			−0.831271	−1.012570	0.500599	0.501957
	3			−0.806517	−1.090060	0.500368	0.502376
	3.5			−0.795918	−1.125350	0.500266	0.502540
	4			−0.786367	−1.158540	0.500172	0.502682
0.3	3	0.3		−0.806517	−1.090060	0.500368	0.502370
		0.7		−0.427685	−0.490977	0.504149	0.504164
		1.3		0.505230	0.598867	0.501464	0.501690
		1.7		1.197720	1.827620	0.497663	0.499169
0.3	3	0.3	0.0	−0.806437	−1.090210	0.500367	0.502377
			0.2	−0.821804	−1.059190	0.500513	0.502218
			0.4	−0.836166	−1.024390	0.500645	0.502024
			0.6	−0.849679	−1.007155	0.500765	0.366731

Table 3
Heat transfer rate $Re^{-1/2}Nu_x$ for different values of β^*, Pr, θ_w, N_R and γ when $M = 0.3$, $\alpha = 0.3$, $Ec = 0.1$ and $We = 3$.

Pr	θ_w	N_R	γ	β^*	$Re^{-1/2}Nu_x$	
					$n = 0.75$	$n = 1.75$
2	1.5	0.7	0.2	0.001	0.273236	0.272824
4					0.266097	0.264471
6					0.258931	0.257190
8					0.253453	0.251803
2	1				0.181550	0.182882
	1.2				0.207981	0.208794
	1.4				0.247517	0.247571
	1.6				0.303518	0.302598
	1.5	1.7			0.435903	0.429010
		2.7			0.576677	0.564581
		3.7			0.711888	0.694991
		0.7	0.4		0.503225	0.511048
			0.6		0.645731	0.663615
			0.8		0.734863	0.760775
			0.2	0.0	0.273236	0.272824
				0.2	0.273218	0.272874
				0.4	0.273201	0.272930
				0.6	0.273184	0.224812
				0.8	0.273168	0.236665

profiles, for both shear thickening $(n > 1)$ and shear thinning $(n < 1)$ fluids. It is observed from these Figs. that increasing the Hartmann number results in diminishing the velocity field and enhancement in temperature field. Physically M shows the ratio of electromagnetic force to the viscous force and strong values of M represents the increase in the Lorentz force. This is drag-like force that creates more resistance to transport phenomenon and fluid velocity as well as boundary layer thickness diminish. Fig. 4 describes the impact of viscosity ratio parameter β^* on velocity $f'(\eta)$ and temperature $\theta(\eta)$ profiles for both hydromagnetic and hydrodynamic cases. It is adequate to note that plots of velocity and temperature uncover inverse pattern with increasing β^*. It is noted that velocity profile depicts a considerable decrease with the higher values of β^* and opposite trend was observed for temperature profile. From Fig. 5, it is seen that increasing values of the n (power law index) expand the fluid velocity for $\alpha < 1$ and opposite trend is observed for $\alpha > 1$. Moreover by increasing the values of power law index n from 0.8 to 1.6 temperature profile decreases, when stretching velocity is greater than the free stream velocity. In addition when $\alpha < 1$ temperature profile decreases.

Fig. 6 is designed to observe the effects of the local Biot number γ and Prandtl number Pr on the temperature profile $\theta(\eta)$ for both the hydrodynamic and hydro magnetic flows. From these Figs, it is observed that stronger values of the Biot number result in higher convection at the stretching sheet which increases the temperature of the fluid. It is also observed that in hydrodynamic flow thermal boundary layer is thicker as compared to hydromagnetic flows. Additionally increasing values of Pr decreases the temperature profile. since the low Prandtl number depicts fluids with high thermal conductivity and this creates thicker thermal boundary layer structures than that for the large Prandtl number. Fig. 7 is a plot of the variation in the temperature distribution for various values of the temperature ratio parameter θ_w and the radiation parameter N_R for both hydrodynamic and hydromagnetic flows. These results reveal that temperature distribution decreases by increasing the values of radiation parameter. The thermal boundary layer thickness contracts for the greater radiation parameter. And the results are totally opposite for the temperature ratio parameter θ_w. The temperature ratio parameter relates to higher wall temperature as compared to ambient fluid and as a result temperature of the fluid increases. Additionally thermal boundary layer thickness rises for higher values of the temperature ratio parameter. Fig. 8 describes the effects of Eckert number Ec on temperature profile $\theta(\eta)$. It is noted that the increasing values of Eckert number flourishes the temperature profile.

Table 2 shows the joint effects of the Hartmann number M and the velocity ratio parameter β^* on the wall shear stress $Re^{1/2}C_{fx}$. Both parameters increase the magnitude of the wall shear stress $Re^{1/2}C_{fx}$ for both shear thinning and thickening fluids. The local skin friction is reduced for the higher values of the Weissenberg number We in the shear thinning fluid and is increased in the shear thickening fluid. Moreover, it is seen that the local Nusselt number $Re^{-1/2}Nu_x$ is decreased with M as the strong magnetic field reduce the extent of heat transfer rate. Table 3 describes the effect of radiation parameter N_R on the local Nusselt number $Re^{-1/2}Nu_x$. The amount of heat transfer rate decreases with the increasing values of N_R. In addition the local Nusselt number increases with strong values of Prandtl number. It is because of the fact that the Prandtl number controls the relative thickness of the thermal boundary layer.

Conclusions

In this article numerical computations for MHD Carreau fluid flow with stagnation point and non-linear radiation over a convectively heated surface have been performed. Numerical results were acquired using RK- Fhelberg method for a number of parameters: the velocity ratio parameter α, Hartmann number M, viscosity ratio parameter β^*, Prandtl number Pr, Biot number γ, temperature ratio parameter θ_w and radiation parameter N_R. The current numerical results were also contrasted and the accessible outcomes were stated with remarkable understanding. The following outcomes can be concluded from the above numerical calculations.

- It was observed that the velocity profile diminished for $\alpha < 1$ and opposite was true for $\alpha > 1$. Moreover temperature profile was decreased for both cases.
- This investigation has explored that an increase in the Hartmann number showed an expansion in temperature of the fluid while an opposite behavior was observed for the fluid velocity.
- The velocity distribution was decreased by increasing viscosity ratio parameter for both hydromagnetic and hydrodynamic flows and quite the opposite was true for temperature distribution.
- Strong Biot number raised the thermal boundary layer thickness.
- Increasing values of Prandtl number decreased the temperature field while temperature flourished for higher values of Eckert number.
- It is important to state that the radiation parameter and temperature ratio parameter predicted the opposite effects on the fluid temperature.

Conflict of interest

The authors have no conflict of interest.

Acknowledgement

The authors wish to express their thanks to the competent reviewers for the valuable comments and suggestions.

References

[1] Pavlov KB. Magneto hydrodynamic flow of an incompressible viscous fluid caused by the deformation of a plane surface. Magnetohydrodynamic 1974;4:146–7.
[2] Andersson HI. MHD flow of a viscoelastic fluid past a stretching surface. Acta Mech 1992;95:227–30.
[3] Makinde OD, Khan WA, Culham JR. MHD variable viscosity reacting flow over a convectively heated plate in a porous medium with thermophoresis and radiative heat transfer. Int J Heat Mass Transfer 2016;93:595–604.
[4] Khan M, Irfan M, Khan WA. Impact of nonlinear thermal radiation and gyrotactic microorganisms on the magneto-Burgers nanofluid. Int J Mech Sci 2017;130:375–82.
[5] Waqas M, Khan MI, Hayat T, Alsaedi A. Numerical simulation for magneto Carreau nanofluid model with thermal radiation: a revised model. Comput Meth Appl Mech Eng 2017;324:640–53.
[6] Khan M, Hussain A, Malik MY, Salahuddin T, Khan F. Boundary layer flow of MHD tangent hyperbolic nanofluid over a stretching sheet: a numerical investigation. Res. Phys. 2017;7:2837–44. https://doi.org/10.1016/j.rinp.2017.07.061.
[7] Sakiadis BC. Boundary layer behavior on continuous solid flat surfaces. J. AICHE 1961;7:26–8.
[8] Crane L. Flow past a stretching plate. Z Angew Math Phys 1970;21:645–7.
[9] Ozisik MN. Interaction of radiation with convection in hand book of single-phase convective heat transfer. New York: John Wiley & Sons; 1987. p. 9.
[10] Nazar R, Amin N, Filip D, Pop I. Stagnation point flow of a micropolar fluid towards a stretching sheet. Int J Non Linear Mech 2004;39:1227–35.
[11] Farooq M, Khan MI, Waqas M, Hayat T, Khan MI. MHD stagnation point flow of viscoelastic nanofluid with non-linear radiation effects. J Mol Liq 2016;221:1097–103.
[12] Cortell R. Heat transfer in a fluid through a porous medium over a permeable stretching surface with thermal radiation and variable thermal conductivity. Can J Chem Eng 2012;90(5):1347–55.
[13] Khellaf K, Lauriat G. Numerical study of heat transfer in a non-Newtonian Carreau fluid between rotating concentric vertical cylinders. J Non-Newtonian Fluid Mech 2000;89:45–61.

[14] Tshehla MS. The flow of Carreau fluid down an inclined with a free surface. Int J Phys Sci 2011;6:3896–910.
[15] Abbasi FM, Hayat T, Alsaedi A. Numerical analysis for MHD peristaltic transport of Carreau-Yasuda fluid in a curved channel with Hall effects. J Magn Magn Mater 2015;382:104–10.
[16] Hossain MA, Alim MA, Rees DAS. Effect of radiation on free convection from a porous vertical plate. Int J Heat Mass Transfer 1999;42:181–91.
[17] Hayat T, Imtiaz M, Alsaedi A, Kutbi MA. MHD three-dimensional flow of nanofluid with velocity slip and nonlinear thermal radiation. J Magn Magn Mater 2015;396:31–7.
[18] Hayat T, Muhammad T, Shehzad SA, Alsaedi A. An analytical solution for magnetohydrodynamic Oldroyd-B nanofluid flow induced by a stretching sheet with heat generation/absorption. Int J Therm Sci 2017;111: 274–88.
[19] Khan M, Hashim. MHD stagnation point flow of a Carreau fluid and heat transfer in the presence of convective boundary conditions. PLoS One 2016;11:157–80.
[20] Khan M, Hashim, Azam M. Magnetohydrodynamic flow of Carreau fluid over a convectively heated surface in the presence of nonlinear radiation. J Magn Magn Mater 2016;412:63–8.
[21] Carreau PJ. Rheological equations from molecular network theories. Trans Soc Rheol 1972;116:99–127.
[22] Rosseland S. Astrophysik und Atom-Theoretische Grundlagen. Springer Verlag 1931:41–4.
[23] Shahzad A, Ali R. Approximate analytic solution for magneto-hydrodynamic flow of a non-Newtonian fluid over a vertical stretching sheet. Can J Appl Sci 2012;2(1):202–15.
[24] Mahapatra TR, Gupta AG. Heat transfer in stagnation point flow towards a stretching sheet. Heat Mass Transfer 2002;38:517–21.
[25] Nazar R, Amin N, Filip D, Pop I. Unsteady boundary layer flow in the region of the stagnation point on a stretching sheet. Int J Eng Sci 2004;42:1241–53.
[26] Ishak A, Nazr R, Pop I. Mixed convection boundary layers in the stagnation-point flow toward a stretching vertical sheet. Meccanica 2006;41:509–18.
[27] Reddy MG, Prasannakumara BC, Makinde OD. Cross diffusion impacts on hydromagnetic radiative peristaltic Carreau-Casson nanofluids flow in an irregular channel. Defect Diffus Forum 2017;377:62–83.
[28] Mamatha SU, Mahesha, Raju CSK, Makinde OD. Effect of convective boundary conditions on MHD Carreau dusty fluid over a stretching sheet with heat source. Defect Diffus Forum 2017;377:233–41.
[29] Makinde OD, Khan WA, Khan ZH. Stagnation point flow of MHD chemically reacting nanofluid over a stretching convective surface with slip and radiative heat. Proc Inst Mech Eng E J Process Mech Eng 2017;231(4):695–703.
[30] Ibrahim W, Makinde OD. Magnetohydrodynamic stagnation point flow of a power-law nanofluid towards a convectively heated stretching sheet with slip. Proc Inst Mech Eng E J Process Mech Eng 2016;230(5):345–54.
[31] Makinde OD, Khan WA, Khan ZH. Buoyancy effects on MHD stagnation point flow and heat transfer of a nanofluid past a convectively heated stretching/shrinking sheet. Int J Heat Mass Transfer 2013;62:526–33.